

University of Nevada, Reno

**Fault Formation in Porous Sedimentary Rocks at High Strain Rates**

A thesis submitted in partial fulfillment of the  
requirements for the degree of Master of Science in  
Geology

by

Wendy R.O. Key

Dr. Richard A. Schultz/Thesis Advisor

May 2009



University of Nevada, Reno  
Statewide • Worldwide

THE GRADUATE SCHOOL

We recommend that the thesis  
prepared under our supervision by

**WENDY R.O. KEY**

entitled

**Fault Formation In Porous Sedimentary Rocks At High Strain Rates**

be accepted in partial fulfillment of the  
requirements for the degree of

**MASTER OF SCIENCE**

Richard A. Schultz, Ph.D., Advisor

John N. Louie, Ph.D., Committee Member

Thomas F. Bullard, Ph.D., Committee Member

Jaak J.K. Daemen, Ph.D., Graduate School Representative

Marsha H. Read, Ph. D., Associate Dean, Graduate School

May, 2009

## ABSTRACT

Previous theoretical work suggests that faults in porous sedimentary rocks subjected to high strain rates do not form from deformation band damage zones (DBDZs) as typically observed in porous rocks. This hypothesis is evaluated by an investigation of faults mapped within the porous Navajo Sandstone at the Upheaval Dome impact structure in Canyonlands National Park, southeast Utah, where high strain rate conditions are known to have occurred. We found no evidence for DBDZ formation along the fault planes at Upheaval Dome. Instead pulverized quartz grains within the Navajo Sandstone are revealed adjacent to several fault planes. This material has previously been observed and documented in association with dynamic fracturing in crystalline and sedimentary rocks along the San Andreas Fault in southern California and in metamorphic rocks along the Bosman fault in South Africa. Additional work has shown that the grain sizes of pulverized rock can be related to the specific strain rate conditions under which pulverization occurred. Measured grain sizes obtained from the pulverized material collected at Upheaval Dome are found to be associated with strain rates of approximately  $10^0$  and  $10^3 \text{ s}^{-1}$ . Previously reported grain sizes for pulverized sedimentary rocks along the San Andreas Fault imply strain rates of approximately  $10^{-2}$  to  $10^1 \text{ s}^{-1}$ . Strain rates at Upheaval Dome are well above the average values associated with intraplate tectonics ( $10^{-20}$  to  $10^{-17} \text{ s}^{-1}$ ), but are consistent with, or somewhat faster than, seismic slip rates along faults such as the San Andreas Fault.

## DEDICATION

This thesis is dedicated to my parents, Keith and Kathy Orr, for making my education possible, and to my husband, Randy Key, for being by my side through it all.

## ACKNOWLEDGMENTS

I would like to thank my advisor, Dr. Richard Schultz for all his guidance and support, and my committee members, Dr. John Louie, Dr. Tom Bullard, and Dr. Jaak Daemen for their comments and additional support. I would also like to thank Dr. Chris Okubo and the Geomechanics-Rock Fracture Group for their assistance in the field and for asking me the hard questions I didn't want to hear. This project was greatly improved by the conversations and suggestions provided by Dr. Ken Herkenhoff, Dr. Ory Dor, Dr. Ze'ev Reches, Dr. Yehuda Ben-Zion, Neta Wechsler, and Dr. Steve Martel. My thanks are also extended to Dr. Anita Torabi for her assistance with the evaluation of my thin sections and to Vicki Webster with the National Park Service for granting field access to Upheaval Dome. This study was supported by a NASA grant provided to Dr. Richard Schultz.

## TABLE OF CONTENTS

	<u>Page</u>
ABSTRACT	i
DEDICATION	ii
ACKNOWLEDGEMENTS	iii
TABLE OF CONTENTS	iv
LIST OF TABLES	v
LIST OF FIGURES	vi
INTRODUCTION	1
FAULTING IN POROUS SEDIMENTARY ROCKS	3
UPHEAVAL DOME	5
Origin	7
Faulting	10
OBSERVATIONS	12
ANALYSIS AND DISCUSSION	21
Grain Size Analysis	21
Strain Rates	24
CONCLUSIONS	29
REFERENCES	31
APPENDIX 1 (Grain Size Measurements)	38
Table A.1	39
Table A.2	43

## LIST OF TABLES

	<u>Page</u>
Table 1      Rock Damage Classifications	18

## LIST OF FIGURES

		<u>Page</u>
Figure 1	Deformation and Faulting in Porous Sedimentary Rocks	4
Figure 2	Location Map and Aerial Photograph of Upheaval Dome	6
Figure 3	Stratigraphic Column of Units Exposed at Upheaval Dome and Younger Eroded Units	8
Figure 4	Deformation Bands and Deformation Band Damage Zones at Upheaval Dome	14
Figure 5	Photograph of Fault 1	17
Figure 6	Undeformed and Pulverized Navajo Sandstone in Thin Section	21
Figure 7	Grain Size Distribution Plot	22
Figure 8	Strain Rate Plot	28

## INTRODUCTION

Several mechanisms for faulting that depend on rock type have been documented in the literature. Better known cases involve faulting of low-porosity crystalline rock such as granite (Lockner et al, 1991; Lockner, 1995). In this case, faulting occurs as a result of either sliding on pre-existing cracks (Segall and Pollard, 1983; Martel and Pollard, 1989) or on damage zones of cracks resulting from shear deformation (Wawersik and Fairhurst, 1970; Wawersik and Brace, 1971, Lockner et al., 1991). In contrast, rocks of high porosity (>5%; Patterson and Wong, 2005), such as sandstones, first generate deformation band damage zones (DBDZs) that subsequently fault (Aydin and Johnson, 1978; Shipton and Cowie, 2001, 2003). This sequence is well documented in rock such as the Navajo Sandstone (Aydin, 1978; Aydin and Johnson, 1978, 1983; Davis, 1999; Davis et al., 1999; Shipton and Cowie, 2001) and the Entrada Sandstone (Aydin, 1978; Aydin and Johnson, 1978, 1983) on the Colorado Plateau as well as other units throughout the world (Fossen et al., 2007). Faulting in porous sedimentary rocks under tectonic conditions is well understood, although faulting in these same rocks at high strain rates has not been studied in the field.

Recent experimental and theoretical work suggests that the formation of deformation bands and DBDZs may depend on the rate of deformation of the host rock (Fossum and Brannon, 2006). Using a combination of viscoplastic computer models and experimental validation (Kolsky bar tests), they find that for the Salem Limestone, compaction-dominated deformation (i.e. deformation bands and DBDZs) typically occurs three times faster than dilation-dominated deformation (i.e. cracking) (Fossum and Brannon, 2006). They showed that compaction-dominated deformation should develop in

the Salem Limestone at strain rates of  $10^{-5} \text{ s}^{-1}$  with cracking-dominated deformation occurring at strain rates of  $10^5 \text{ s}^{-1}$ . This intriguing and novel result suggests that a transition from compaction-dominated deformation (DBDZs) to cracking-dominated deformation in other porous rock types, such as the Navajo Sandstone and the Entrada Sandstone, may also form under a particular range of strain rates.

To evaluate the mechanics of faulting in porous sedimentary rocks subjected to high strain rates we focused on macroscopic and microscopic data collected in the field along faults inferred to have formed under these conditions. The Upheaval Dome impact structure was chosen for this investigation because high strain rate conditions are known to have been applied at this location during impact and faults associated with the impact event are well documented (Kriens et al, 1997, 1999; Kenkmann et al, 2005). Rock units affected by the impact and preserved within the perimeter of Upheaval Dome include the porous Navajo Sandstone, which provides an ideal lithology for comparing the mechanics of fault formation observed on the Colorado Plateau to those generated during a high strain rate impact event. We find that DBDZs do not form at high strain rates in the Navajo Sandstone at Upheaval Dome and instead a cracking-dominated behavior generating pulverized rock occurs. Using the measured grain sizes of the pulverized rock, strain rates under which this material formed are calculated and compared to additional pulverized rock data that has been collected along the Mojave section of the San Andreas Fault in southern California (Dor et al., 2009).

## **FAULTING IN POROUS SEDIMENTARY ROCKS**

The process leading to fault formation in porous sedimentary rocks has been extensively studied, particularly within the Colorado Plateau of the western United States (Aydin, 1978; Aydin and Johnson, 1978, 1983; Davis, 1999; Davis et al., 1999; Shipton and Cowie, 2001, 2003; Schultz and Balasko, 2003; Schultz and Siddharthan, 2005; Schultz and Okubo, 2005; Fossen et al., 2007). In porous granular rocks, such as sandstones, deformation bands and DBDZs (i.e. compaction-dominated deformation) are often observed in association with larger offset faults (Aydin and Johnson, 1978, 1983; Davis, 1999, Shipton and Cowie, 2001, 2003). Deformation bands are defined as tabular discontinuities within a porous granular rock that accommodate strain through compaction, dilation, shear, or a combination of these (Antonellini et al., 1994; Aydin et al., 2006; Schultz and Fossen, 2008). Deformation bands are commonly millimeters in width and accommodate shear displacement on the order of millimeters to centimeters (Aydin, 1978; Aydin and Johnson, 1978). As shown in Figure 1A and 1B, compactional and cataclastic deformation bands typically display strain-hardening and are therefore more resistant to erosion (Aydin, 1978).

In thin section, deformation bands are characterized by an “inner zone” of intensely fractured and crushed grains (Aydin, 1978) and an “outer zone” in which pore space is decreased and grain-to-grain contact is increased (porosity reduced to  $\leq 10\%$ ; Aydin, 1978) surrounded by undeformed rock (Aydin, 1978; Aydin and Johnson, 1978; Fossen et al., 2007). Primary mechanisms for the formation of deformation bands are the closing and collapsing of pore space within the rock, microfracturing, and rotation of the grains (Aydin, 1978).



Figure 1: Deformation and faulting in the porous Entrada Sandstone located near the San Rafael Swell in southern Utah. A. Several individual deformation bands. B. A DBDZ with linking geometries visible in cross-section. Note that deformation bands in both A and B display strain hardening and positive relief in comparison to the surrounding, undeformed Entrada Sandstone. C. A normal fault with several meters of offset cutting the Entrada Sandstone above and the Carmel Formation below. The fault is shown cutting through a DBDZ that is approximately 3 meters in width.

Due to the increased strength of the sandstone as a result of reduced porosity and strain-hardening (Aydin, 1978), further deformation within a porous rock is accommodated by the formation of additional parallel or subparallel deformation bands (Aydin and Johnson, 1978). The presence of two or more parallel or subparallel individual deformation bands defines a DBDZ (Aydin and Johnson, 1978). DBDZs characteristically display a lenticular or wavy pattern when observed in the field in plan view (Aydin, 1978; Aydin and Johnson, 1978; Schultz and Balasko, 2003) and a backward-breaking linking geometry in cross-section (Davis, 1999; Schultz and Balasko, 2003). An oblique image of a DBDZ in the Entrada Sandstone is shown in Figure 1B and

displays the geometry of the zone in both plan view and cross-section. DBDZs are typically on the order of decimeters to meters in thickness (Aydin and Johnson, 1978; Shipton and Cowie, 2001; Schultz and Siddharthan, 2005), however thicknesses vary depending on the number of deformation bands within a zone and the width of the undeformed rock lenses between each of the bands (Aydin and Johnson, 1978). The total amount of offset accommodated by a DBDZ is determined by summing the displacements of each individual deformation band within the damage zone resulting in offsets up to several centimeters (Aydin and Johnson, 1978).

To accommodate larger displacements on the order of decimeters to meters, a transition from a zonal-style of deformation within the DBDZ occurs and a slip-surface, or fault, forms (Aydin and Johnson, 1978, 1983). This transition occurs where the mechanical strength between the individual strain-hardened deformation bands comprising the DBDZ and the adjacent porous, relatively undeformed rock fails (Aydin and Johnson, 1983). In Figure 1C, a fault formed by failure within a DBDZ offsetting several meters of the Entrada Sandstone and Carmel Formation is shown. Although faults within porous sedimentary rock are commonly associated with deformation bands and DBDZs, deformation bands and DBDZs can occur in isolation and are not unique indicators of fault formation (Aydin and Johnson, 1978).

## **UPHEAVAL DOME**

An impact structure is an ideal location to evaluate fault formation at high strain rates in porous sedimentary rocks where cracking-dominated deformation (i.e. dilational-style deformation) is likely to occur as a result of the very high stresses applied. Impact

structures are known to form as a result of average strain rates in excess of  $10^{-2}\text{s}^{-1}$  (Melosh, 1989; Pati and Reimold, 2007). Upheaval Dome is a circular structure approximately 5.5 km in diameter located on the Colorado Plateau in southeastern Utah (Figure 2) and is estimated to be Jurassic (Alvarez et al., 1998) or Cretaceous (Kenkmann et al., 2005) in age.

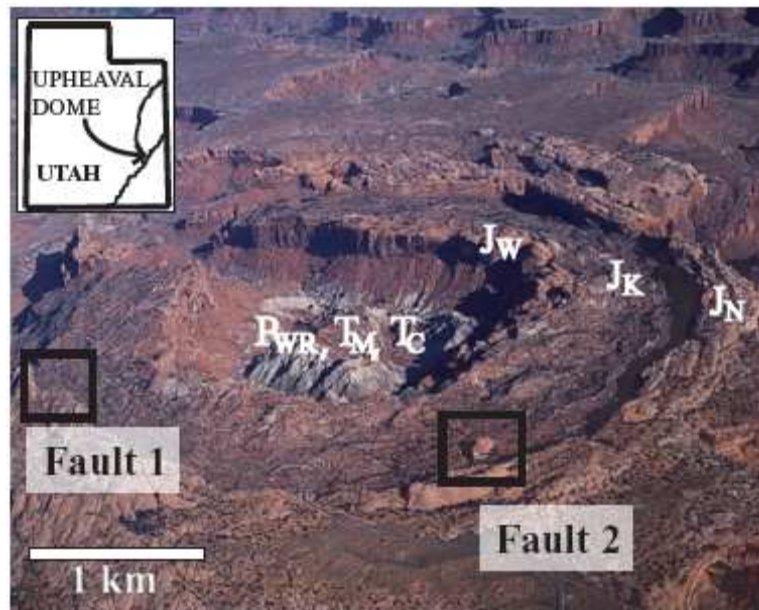


Figure 2: An oblique aerial view of the Upheaval Dome impact structure located in southeast Utah (see inset location map in the upper left corner). The central uplift is characterized by the light-colored rocks mounded in the center of the crater and is composed of the White Rim Sandstone ( $P_{WR}$ ) and the Moenkopi ( $T_M$ ) and Chinle ( $T_C$ ) Formations. The rim syncline is composed of the cliff-forming Wingate Sandstone ( $J_W$ ) located outside the central uplift, the topographic low formed by the Kayenta Formation ( $J_K$ ), and another cliff-forming unit, the Navajo Sandstone ( $J_N$ ), located along the perimeter of the crater. The rim monocline extends outward from the Navajo Sandstone to the flat lying strata surrounding the impact structure. The locations of the faults evaluated in this study, Fault 1 and Fault 2, are shown within the Navajo Sandstone of the rim syncline (photograph courtesy of Tom Till Photography, Moab, Utah).

Structurally, Upheaval Dome is characterized by a complex central uplift, a rim syncline, and an outer monocline dipping away from the center of the structure (Shoemaker and Herkenhoff, 1983; Kriens et al., 1997, 1999; Jackson et al., 1998). The

structurally complex central uplift at Upheaval Dome has been attributed to the gravitational collapse of the transient (bowl-shaped) crater formed during the initial stages of the impact event (Shoemaker and Herkenhoff, 1983; Melosh, 1989) and has led to the classification of Upheaval Dome as a complex impact crater (Shoemaker and Herkenhoff, 1983; Kriens et al., 1997, 1999). A stratigraphic sedimentary sequence composed of the Permian White Rim Sandstone of the Cutler Group, Triassic Moenkopi and Chinle Formations, and Jurassic Wingate Sandstone, Kayenta Formation, and Navajo Sandstone is exposed within the structure (refer to Figure 3). We selected Upheaval Dome for this investigation because the lithologies exposed at this structure include the same lithologies (i.e. the Navajo Sandstone) in which faulting has been studied on the Colorado Plateau. The Navajo Sandstone in particular is an ideal lithology for evaluating the mechanics of faulting at high strain rates because it provides an opportunity to make mechanical comparisons to compactional deformation documented throughout the Colorado Plateau (Aydin, 1978; Aydin and Johnson, 1978; Davis, 1999; Shipton and Cowie, 2001, 2003).

### *Origin*

For decades, the origin of Upheaval Dome had been a source of debate, however in recent years the theories for its formation have focused on salt intrusion or meteorite impact. According to the salt intrusion hypothesis, Upheaval Dome was formed by upward migration of salt from the underlying Paradox Formation which has been regionally identified as the source of numerous salt structures throughout the area (Harrison, 1927; McKnight, 1940; Mattox, 1975). Schultz-Ela (1994) and Jackson et al.

Age	Thickness (in meters)	Unit Description	Additional Comments
Jurassic		J <sub>E</sub> Entrada Sandstone- Light to red, usually massive sandstone. (Not drawn to scale.)	Deformation bands (Jurassic) documented in the J <sub>E</sub> at Arches National Park.  Deformation bands (late Cretaceous to late Paleogene) documented in the J <sub>N</sub> in western Utah.  Deformation bands (post-early Jurassic) documented in the J <sub>W</sub> at Upheaval Dome.
		J <sub>C</sub> Carmel Formation- Red sandstone, siltstone, and shale with basal limestone. (Not drawn to scale.)	
	900	J <sub>N</sub> Navajo Sandstone- Porous, highly cross-bedded buff to red sandstone.	
	800	J <sub>K</sub> Kayenta Formation- Red, gray, and purple shale and sandstone.	
	700	J <sub>W</sub> Wingate Sandstone- Massive, red, cliff-forming sandstone.	
	600	T <sub>C</sub> Chinle Formation- Partly silty and sandy variegated shales, with thin limestone and conglomerate lenses.	
Triassic	500	T <sub>M</sub> Moenkopi Formation- Primarily red to brown shale, siltstone, and sandstone with gray limestone interfingering.	
	400		
Permian	300	P <sub>WR</sub> Cutler Group- Red arkosic sandstone and conglomerate, sandy shale, and limestone. White Rim Sandstone observable at the top of the section.	Units exposed within Upheaval Dome
	200	P <sub>C</sub>	
	100		
	0		

Figure 3: Stratigraphic column of units exposed at Upheaval Dome and younger eroded units after Jackson et al. (1998) (data from the Buck Mesa #1 well log, Fiero [1958], Mattox [1968], and Woodward-Clyde Consultants [1983]). Unit descriptions shown above are from Molenaar (1975). Comments regarding observed deformation bands and the ages of deformation are from Antonelli et al. (1994) (Entrada Sandstone), Davis et al. (1999) (Navajo Sandstone), and Okubo and Schultz (2007) (Wingate Sandstone).

(1998) suggested that a pinched-off salt diapir had passed through Upheaval Dome's center and had subsequently been eroded away. Using structural and stratigraphic relationships, Jackson et al. (1998) suggested that Upheaval Dome underwent prolonged growth beginning in the Jurassic that continued for ~ 20 million years. They cited a concentric fold system composed of an outer rim monocline, a rim syncline, and an inner dome as geomorphic evidence for salt diapirism (Jackson et al., 1998). Additional evidence cited in favor of salt diapirism was syndimentary deformation (i.e. truncations, channels, and growth folds) within the Chinle Formation, Wingate Sandstone, and Kayenta Formation, and emplacement of the clastic dikes along faults inferred to have formed in the neck of the pinched-off salt structure (Jackson et al., 1998).

Significant evidence supporting an impact origin for the structure has shown that Upheaval Dome is instead a deeply eroded impact crater. Shocked quartz grains (i.e. "the smoking gun") have been obtained and identified in interbedded sandstone units within Kayenta Formation of Upheaval Dome's rim syncline (Buchner and Kenkmann, 2008). Shocked quartz is known to form as a result of shock impact and is an undisputed indicator of an impact origin (Ashworth and Schneider, 1985; Gratz et al., 1988; French, 1998).

Huntoon (2000) presented a compilation of identified strain indicators documented at Upheaval Dome to show the structure's morphology is consistent with proven impact craters rather than salt intrusion. To do so, he categorized observed indicators with the excavation (initial formation) and modification (collapse) phases of crater formation as defined by Melosh (1989). Citing the presence of cataclastic dikes, pseudo-shatter cones, and mechanical (i.e. thrust faulting) and ductile thickening

structures within the Wingate Sandstone, Huntoon (2000) correlated these features with the excavation phase of crater formation. Evidence for the modification phase include the presence of a central uplift peak, outwardly plunging anticlines, mechanical thinning resulting in the formation of a ring syncline, imbricated thrust sheets, and listric normal faults (Huntoon, 2000).

Seismic reflection studies conducted through the structure have revealed that deformation decreases with depth and layers above the Paradox Formation are relatively flat lying, favoring an impact origin for Upheaval Dome and contradicting the salt intrusion model (Louie et al., 1995; Kanbur et al., 2000). Additional evidence supporting an impact origin for Upheaval Dome includes morphology and structural geology consistent with an impact structure (i.e. central uplift, rim syncline, and rim monocline [(Shoemaker and Herkenhoff, 1983; Kriens et al., 1997, 1999)], fault kinematics (Kenkmann et al., 2005), and microstructures such as cataclastic dikes (Kenkmann, 2003) and compactional deformation bands in the Wingate Sandstone (Okubo and Schultz, 2007). Based on the evidence summarized above, Upheaval Dome is best interpreted as an eroded complex impact crater and faults mapped within the structure were formed in response to high strain rates generated during a hypervelocity impact event.

### *Faulting*

The majority of terrestrial impact research has been focused on crater morphology (Shoemaker, 1960; Melosh and Gaffney, 1983; Melosh, 1989; Grieve, 1991; Morgan and Warner, 1999; Grieve and Therriault, 2003), geochemical characteristics such as the presence of high temperature and high pressure minerals and shock (or planar)

deformation features in quartz and feldspars (Grieve and Therriault, 2003; Osinski and Spray, 2005; Kenkmann, 2008), and shatter cones (Sagy et al., 2002, 2004; Grieve and Therriault, 2003; Pati and Reimold, 2007). In contrast, studies of faulting at impact craters are less common. For example, Spray (1997) identified faults at impact craters as “superfaults”, or faults that accommodate very large displacements ( $\geq 100$  m) during single slip events in which velocities greater than 0.1 m/s occur. Although impact events are known to form “superfaults”, these faults are not unique to impact craters and are also documented in association with landslides and the collapse of caldera craters (Spray, 1997).

Detailed structural mapping studies have been conducted at Upheaval Dome in the United States (Kriens et al., 1997, 1999; Kenkmann et al., 2005) and Haughton crater in Canada (Osinski and Spray, 2005) resulting in fault kinematics that has been well-documented at these locations. Structural and stratigraphic mapping at Upheaval Dome has been conducted by Kriens et al. (1997, 1999) and in the central uplift by Kenkmann (2003), Kenkmann et al. (2005), and Scherler et al. (2006). Using a three dimensional (3D) visualization model (3D-Move), Kenkmann et al. (2005) evaluated the geometry of faults and strata within the central uplift at Upheaval Dome in order to better understand its deformational history. They found imbricated thrust slices are prominent in the central uplift with localized faulting common in stratified siliciclastic rocks and non-localized cataclastic flow dominant in massive sandstones (Kenkmann et al., 2005). Thrust faults with offsets ranging from 5 to 500 m are associated with structural thickening at Upheaval Dome and are prevalent within the central uplift of the structure (Kriens et al., 1999; Kenkmann et al., 2005) and listric normal faults associated with structural thinning

are documented in the ring syncline of the crater (Kriens et al., 1999). In the field, offset bedding, drag folds, and fault striae have been used to infer inward radial vergence for normal faults and most thrust faults, with displacement along some concentric (circular) thrust faults (Kriens et al., 1999).

Detailed mapping studies at Haughton crater on Devon Island, Canada (Osinski et al., 2005; Osinski and Spray, 2005) have also resulted in well-documented fault kinematics. Rocks affected by impact at Haughton crater include limestones, dolomites, evaporates and shales ranging from Ordovician to Silurian in age (Osinski et al., 2005; Osinski and Spray, 2005). Osinski and Spray (2005) have attributed observed sub-vertical radial faults and fractures, sub-horizontal bedding-parallel detachment faults, and minor concentric faults and fractures to the excavation phase of crater formation. Major listric faults, antithetic faults and collapse grabens, as well as additional sub-vertical radial faults and fractures with some oblique strike-slip motion are inferred to have developed during the modification stage (Osinski and Spray, 2005). Fault studies comparable to those conducted on the Colorado Plateau are not currently available for rocks located on Devon Island surrounding Haughton crater, therefore we chose to evaluate faulting at Upheaval Dome for this study. To date, an evaluation of the mechanics of faulting in high porosity rocks under impact conditions is not available.

## **OBSERVATIONS**

Faults investigated in this study were identified at Upheaval Dome using the geologic map published by Kriens et al. (1999) and were limited to faults within the Navajo Sandstone, a porous, quartz-rich, cross-bedded sandstone unit and the underlying

Kayenta Formation (see Figure 3). Fault 2 has been mapped as a thrust fault (Kriens et al., 1999), however to date the kinematics at Fault 1 have not been documented. Evidence for the mechanics of fault formation is best preserved at fault tips where the offsets are smallest (Crider and Peacock, 2004), therefore we chose to focus on faulting observed within the rim syncline. Faults in the central uplift of the crater where faulting of finer-grained strata with large offsets is pervasive, and individual, continuous faults are difficult to identify, have been excluded from this study. Two faults, Fault 1 and Fault 2, were chosen for detailed study based on their locations and accessibility (Figure 2). Faults observed in association with the impact at Upheaval Dome are known to have formed during a single event with no significant offset occurring along the faults subsequent to crater formation. Such conditions are ideal, as the evidence for fault formation will be preserved in its original form with no additional deformation or overprinting obscuring mechanical observations.

Compactional (cataclastic) deformation bands of post-early Jurassic age have previously been documented at Upheaval Dome in the Wingate Sandstone, and based on calculated stress magnitudes of  $\geq 0.7$  GPa, the deformation bands have been attributed to the formation of Upheaval Dome during an impact event (Okubo and Schultz, 2007). During our investigation, deformation bands were also observed throughout the Navajo Sandstone in the rim syncline. The deformation bands were observed to be millimeters in width and occasionally accumulated into small DBDZs on the order of several centimeters in width as shown in Figure 4. Observed deformation bands and DBDZs within the Navajo Sandstone exhibit no evidence (i.e. slip surfaces) for faulting.

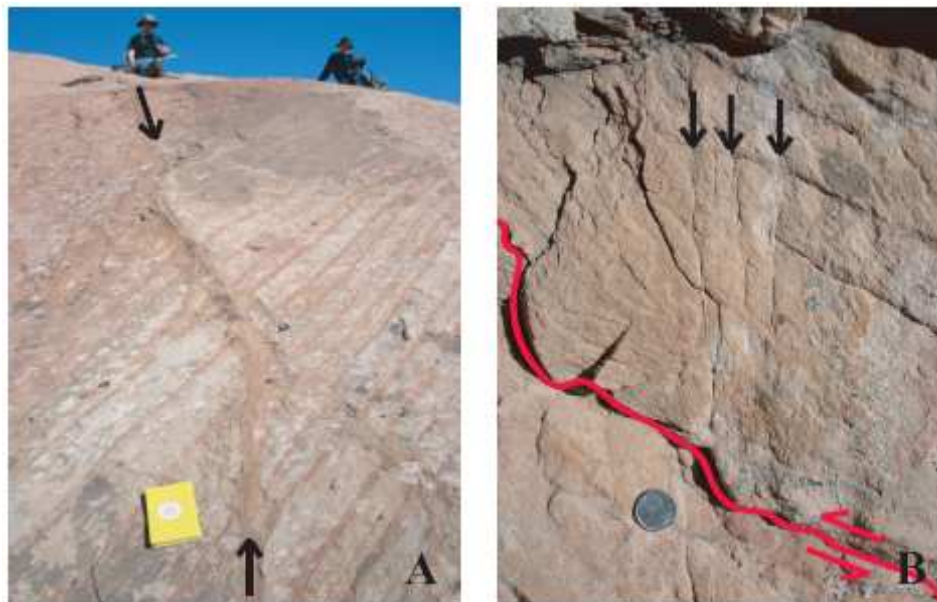


Figure 4: Deformation bands within the Navajo Sandstone at Upheaval Dome. A. A small DBDZ (~ 5 cm in width) observed in the southeastern portion of the crater rim. Arrows mark the alignment of the DBDZ and distinguish it from the cross-bedding typical of the undeformed Navajo Sandstone. B. Three individual deformation bands (~ 1 mm in width) observed perpendicular to Fault 2 (a thrust fault with the fault plane and motion indicated by the red line and arrows). The thicknesses of the bands decrease with proximity to the fault.

At Fault 1 and Fault 2, we observed some additional deformation bands, but no occurrences of DBDZs like those found in the same rock types (i.e. Navajo Sandstone and Entrada Sandstone) outside the Upheaval Dome structure on the Colorado Plateau. As shown in Figure 4B, the bands observed next to the faults evaluated did not accumulate into DBDZs and are typically oriented perpendicular to the fault planes. The thicknesses of the deformation bands were approximately 1 mm with a visible reduction in thickness with proximity to the faults. We infer that the faults evaluated in this study are not related to the adjacent deformation bands within the Navajo Sandstone and were therefore not generated as a result of compaction-dominated deformation as typically observed throughout the Colorado Plateau. If the deformation bands perpendicular to the

faults had existed before impact, we would expect to find the bands maintaining a relatively constant thickness abutting the fault plane and the bands offset by movement along the fault. Had the bands formed as a direct result of impact, we anticipate the deformation bands would have formed parallel or subparallel to the fault plane. Therefore we suggest the deformation bands observed within the Navajo Sandstone formed independently after the impact event.

Although Okubo and Schultz (2007) attributed compaction bands observed within the Wingate Sandstone to an impact event at Upheaval Dome, they showed the observed compaction bands did not form through-going faults in the Wingate Sandstone. Okubo and Schultz (2007) also showed that the compaction bands formed during the initial compaction stage of impact and not during the subsequent excavation and modification stages during which faulting typically occurs (Melosh, 1989). In the Cottonwood area of the Kaibab Uplift and the Sheets Gulch area between the Circle Cliffs and Miners Mountain Uplifts in western Utah, deformation bands and DBDZs have been documented in the upper Navajo Sandstone and are believed to have formed in response to Laramide (late Cretaceous to late Paleogene) uplift on the Colorado Plateau (Davis et al., 1999). It is possible that the deformation bands and DBDZs observed in eastern Utah may also have formed in response to the stresses applied during the Laramide. Deformation bands and DBDZs in closer proximity to Upheaval Dome have also been documented in Arches National Park in units ranging from the Chinle Formation to the Entrada Sandstone (Antonellini et al., 1994). Here Antonellini et al. (1994) have suggested that the deformation bands and DBDZs likely formed in two stages during the Jurassic, first in response to upward salt movement followed by the subsequent dissolution of salt within

the salt-cored anticline. No measurements were made regarding the orientations of the deformation bands and DBDZs at Upheaval Dome during this investigation, therefore an origin for the stresses resulting in this deformation cannot be determined. Because DBDZs were not observed in association with the faults within the Navajo Sandstone at Upheaval Dome, we infer that the faults were formed by a mechanism different from that identified elsewhere on the Colorado Plateau (i.e. compaction-dominated deformation).

Instead of faulted DBDZs, we observed a friable rock with a powdery texture along the fault planes. At Fault 1, this rock is white in color and approximately 2 to 6 cm thick. At Fault 2, the rock is tan in color and approximately 2 to 3 cm thick. At both faults, the Navajo Sandstone is observed above the fault and sheared Kayenta Formation is observed below; no parallel DBDZs are observed adjacent to either fault in the Navajo Sandstone as would be the case elsewhere on the Colorado Plateau in these units. The friable rock was identified as deformed Navajo Sandstone based on field relationships shown in Figure 5, in which it was consistently observed between the fault plane and relatively undeformed Navajo Sandstone. Thin section observations were also used to identify this material as Navajo Sandstone (i.e. quartz-rich, high porosity). Iron oxidation coating the quartz grains was noted in the thin section for the friable rock collected along Fault 2, and likely is responsible for the tan color observed. The deformed Navajo Sandstone was distinctly different from typical outcrops of tan and consolidated, relatively undeformed Navajo Sandstone observed elsewhere throughout the impact structure (see Figures 4 and 5). Preferential weathering resulting in the formation of caves, as shown in Figure 5, and planar gaps within the host rock is noted in association with the fault planes in which the friable rock was documented.

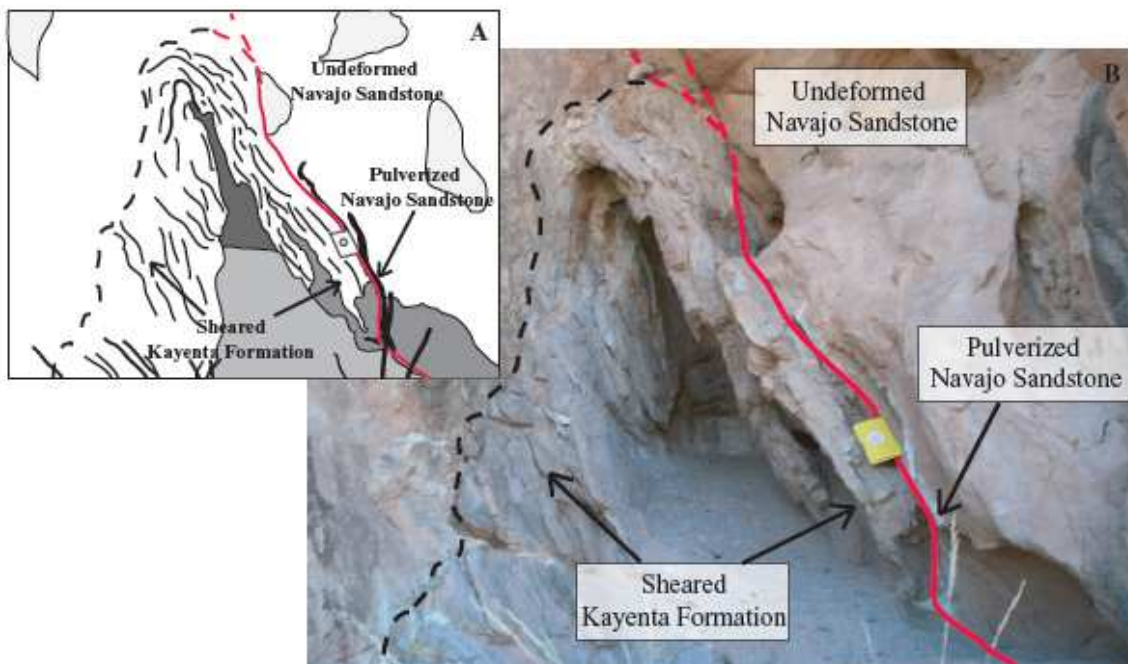


Figure 5: Fault 1 (fault plane shown in red) as observed in the field with a cave formed likely due to preferential weathering of fault rock. Undeformed Navajo Sandstone surrounds the deformed fault rocks characterized by pulverized sandstone and sheared siltstone. A. A schematic diagram of Fault 1 with pulverized Navajo Sandstone shown in black just above the fault plane. B. A photograph of Fault 1 oriented facing south and away from the center of the crater. Pulverized Navajo Sandstone is shown as the thin white unit (2 to 6 cm in width) to the right of the field notebook and above the fault. In both A and B, sheared siltstone of the Kayenta Formation is observed beneath the fault plane and to the left of the notebook. The Kayenta Formation and Navajo Sandstone contact left of the main fault plane is shown by the dashed line on the left of the cave.

We interpret the friable rock observed along fault planes at Fault 1 and Fault 2 as “pulverized” Navajo Sandstone, a material consistent with cracking-dominated deformation. Pulverized rock is defined by Dor et al. (2006) and Dor (2007) as rock that typically yields a white, powdery texture in the field and is observed in thin section to be shattered in place to the microscale maintaining its original grain fabric with little to no evidence for rotation or shear after fragmentation. Five damage classes distinguishing the intensities of fractured rock (including pulverized rock) have been identified (Dor et al.,

Damage Class		Description
I	Weak fracturing	Rock with large macroscopic fractures exceeding background fracture density.
II	Fragmentation	Rock that is fragmented with cm-scale fractures. Rock yields a rugged appearance with fragments that can be crushed to smaller pieces by hand.
III	Intense fracturing	Rock fractured at the grain-scale. Rock yields a texture similar to grus and is characterized by rough, rounded surfaces.
IV	Weak/selective pulverization	Rock with grains fractured to the microscale. Some crystals or grains remain intact, some break along sub-crystal or grain fractures, and some yield a powdery texture. Rock is easily eroded with smooth and rounded outcrops.
V	Pervasive pulverization	Rock with grains fractured to the microscale. All crystals or grains yield a powdery texture when crushed by hand. Rock is easily eroded with smooth and rounded outcrops.

Table 1: Summary of damage classes ranging from degrees of fragmentation/fracturing (Classes I-III) to degrees of pulverization (Classes IV and V) as identified by Dor et al. (2006) along the Mojave section of the San Andreas Fault in southern California. Damage classes are determined by the intensity of observed deformation in proximity to faulting and range from weak fracturing at the macroscopic scale to pervasive pulverization at the microscopic scale (Dor et al., 2006; Dor, 2007).

2006; Dor, 2007) and are summarized in Table 1. Damage along a fault plane has been shown to be asymmetric, with increased damage on the stiffer side of the fault where a higher seismic velocity is obtained during dynamic rupture (Dor et al., 2006, 2009). This is consistent with our observations at Upheaval Dome in which we find rock pulverization in the stiffer Navajo Sandstone above the fault plane and shear deformation in the softer clay and siltstone units of the Kayenta Formation below the fault plane. Pulverized rock along a fault is now recognized as distinct from gouge (Brune, 2001; Dor et al, 2006, 2009; Dor, 2007), which requires shearing and grain flow to form (Engelder, 1974), and is considered to be diagnostic of high-velocity slip events along a fault (Brune, 2001; Dor et al., 2006, 2009; Dor, 2007; Wilson et al, 2005; Reches and Dewers, 2005).

Current research on high strain-rate faulting has linked dynamic slip events to pulverization in a variety of rocks types ranging from granite to porous sandstones at the San Andreas Fault (Brune, 2001; Dor et al., 2006, 2009; Dor, 2007) and quartzites at the Bosman fault (Wilson et al, 2005; Reches and Dewers, 2005). Prior to this investigation, pulverized rock had not been identified or documented along faults within an impact structure. Although the origin of pulverized rock is not well understood, the structural context in which it is observed indicates a clear association with seismogenic faulting (Prakash et al., 2008). Two mechanisms have been proposed for the formation of pulverized rock including a localized reduction in fault-normal stress during rupture passage (Brune, 2001; Wilson et al., 2005; Dor et al., 2006) or pulverization due to changing stress conditions localized at the rupture tip during earthquake propagation (Reches and Dewers, 2005; Wilson et al., 2005).

Analysis of pulverization in porous sedimentary rocks such as those found in the Juniper Hills and the Hungry Valley Formations along the San Andreas Fault suggests that the upper bound for rock pulverization is limited to the top 1 to 3 km of earth's crust (Dor et al., 2009). This inference is supported by poor consolidation and an abundance of open fractures observed within the Juniper Hills and Hungry Valley Formations suggesting that neither formation has been subjected to high confining stresses that would indicate deep burial (Dor et al., 2009). Field studies by several research groups worldwide are demonstrating that material along some major faults may be pulverized rock, instead of gouge as had previously been mapped or inferred (Brune, 2001; Dor et al, 2006), with important revised implications for the mechanical behavior of the faults.

In thin section pulverized rock differs significantly from fault gouge (Engelder, 1974) or compaction bands (Holcomb et al, 2007; Schultz and Fossen, 2008) by the lack of rotation or shear of the grains after fragmentation. Gouge zones are typically characterized by the development of several different shear planes including en échelon  $R_1$ -shears, conjugate  $R_2$ -shears, antithetic P- and X-shears, and Y-shears parallel to country rock interfaces (Gu and Wong, 1994). Laboratory experiments evaluating the formation of gouge in coarse quartz grains (median particle size of  $2.5 \times 10^{-5}$  m) have shown that compactive grain crushing inhibits shear localization and results in homogeneous cataclastic flow (Gu and Wong, 1994). Only after sufficient compaction and grain-size reduction had occurred was shear localization observable in the coarse-grained gouge (Gu and Wong, 1994). Fault material observed along Fault 1 and Fault 2 displayed no evidence for shear localization or cataclastic flow after fragmentation, and is therefore consistent with pulverized rock and not gouge.

Varying degrees of pulverization within the Navajo Sandstone along faults at Upheaval Dome were observed in thin section with the highest degree of pulverization observed at Fault 1 (Figure 5) when compared to rock at Fault 2 and the undeformed Navajo Sandstone. Although grain rotation may have occurred during fault formation, any observable rotation or shear is much less than the grain sizes observed. As shown in Figure 6, pulverized grains observed in thin section have clearly been shattered yet maintain their original grain boundaries. Shattered clasts within these grains have been visibly reduced to the microscale with grain sizes ranging from  $3.75 \times 10^{-6}$  m to  $1.40 \times 10^{-4}$  m. Thus weak/selective pulverization, in which some grains remain intact while others shatter, is identified in thin section along faults at Upheaval Dome (corresponding

approximately with damage class IV as defined by Dor et al., 2006 and Dor, 2007; Table 1).

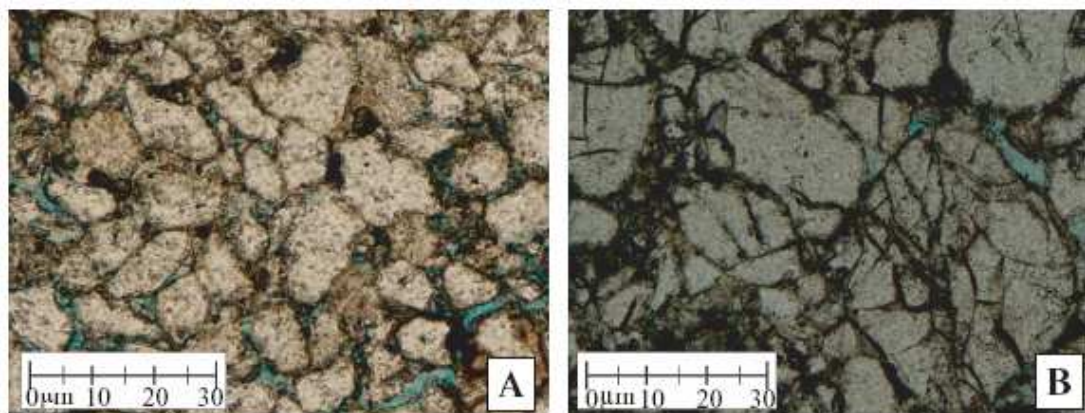


Figure 6: Photographs of quartz grains in the undeformed Navajo Sandstone (A) and pulverized Navajo Sandstone (B). A. Grains shown in the undeformed rock are sub-angular to sub-rounded and display little to no fracturing. B. By contrast, the grains shown in the pulverized rock display significant fracturing. Also note, there is no significant evidence for rotation or shear and the rock maintains its original fabric (i.e. rock fabric and grain organization is the same as that presented by the undeformed rock in A). Images of thin sections recorded at 10x magnification, plane-polarized light. Pore space in each section is represented by blue epoxy.

## ANALYSIS AND DISCUSSION

### *Grain Size Analysis*

Several different methods have been employed to evaluate the reduced grain sizes of fault rocks including water disaggregation (An and Sammis, 1994; Reches and Dewers, 2005), sieve analysis (An and Sammis, 1994), Coulter-Counter analysis (An and Sammis, 1994), and digital analysis of grain perimeter ratios from thin section images (Dor, 2007, Dor et al., 2009). For this study, we chose to measure grain sizes directly from images taken from thin section. This method has been used in the evaluation of grain size reduction within deformation and compaction bands (Sternlof et al., 2005; Torabi et al., 2007) and displays the grain sizes and packing conditions as they exist in the field.

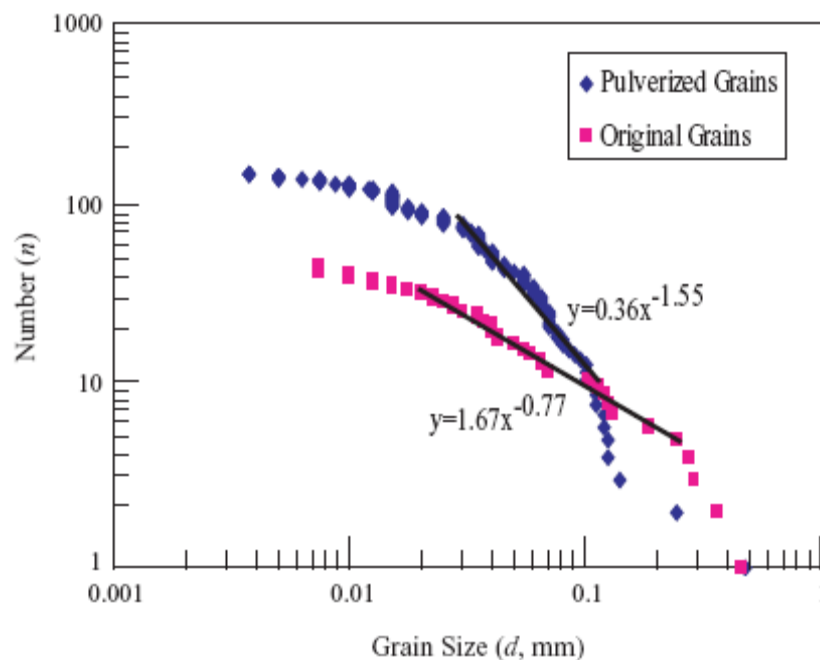


Figure 7: Log-log plot comparing pulverized grain sizes and original grain sizes measured in thin section. The regression lines in each data set were used to determine the power law governing grain size and were obtained by removing data outliers. A power law slope of 1.55 was obtained for the pulverized grains and a power law slope of 0.77 was obtained for the original grains.

Figure 7 presents a log-log plot of measured grain sizes collected from the thin section of the pulverized rock at Fault 1 (see Figure 6) and the power law distribution of the pulverized rock compared to the original grain sizes. Grain sizes obtained from the pulverized rock (i.e. individual grain fragments) have a larger concentration of microscale grain fragments than the undeformed rock (i.e. original grains). Although the regression lines shown in Figure 7 have a negative slope, the power law is reported as positive value by convention to allow for more direct comparisons to previous work evaluating the grain size distribution of fault gouge (An and Sammis, 1994; Sammis and Steacy, 1995; Sammis and King, 2007).

We obtain a two dimensional (2D) power law slope of 0.77 for the original grain sizes and 1.55 for the pulverized grain sizes collected from Upheaval Dome. We find that the power law slope obtained for the pulverized grain fragments is twice as large as the power law slope that is obtained for the original grains, however it is not clear if this relationship is significant. The 1.55 power law slope obtained from the pulverized grain sizes is remarkably close to the 1.6 2D slope obtained from fault gouge reported by Sammis et al. (1987) and Sammis and Steacy (1995). It has been suggested that the distribution of grain size within fault gouge can be correlated to strain rate conditions (Sammis et al., 1987; An and Sammis, 1994; Sammis and Steacy, 1995; Sammis and King, 2007, etc.) Smaller grain sizes ( $\geq 0.1$  mm) with a 2D power law slope of 2.0 have been reported in association with higher strain rates and larger grain sizes ( $\leq 0.001$  mm) with a 2D power law slope of 2.6 associated with “low-strain gouge” (Sammis and King, 2007). The pulverized rock collected at Upheaval Dome is inferred to have formed in a high strain rate environment, however the power law slope associated with our pulverized grain sizes matches the 1.6 2D power law slope for “low-strain gouge and breccia” reported by Sammis et al. (1987) and Sammis and Steacy (1995). Our data suggest a degree of non-uniqueness in grain size distributions of pulverized rock and fault gouge. Comparable studies using the method employed in this investigation (i.e. direct thin section measurements) for the evaluation of pulverized rock are not available in the literature, so we rely on observable traits in the field and in thin section to distinguish pulverized rock from fault gouge rather than the grain size distribution alone.

### *Strain Rates*

Results from laboratory and controlled blasting experiments used to evaluate dynamic fragmentation in rock have defined a relationship between grain size and the strain rate responsible for the observed grain size reduction (Grady and Kipp, 1987; Zhou et al., 2005). Blasting experiments were conducted within oil shales in Rifle, Colorado in order to prepare the rock for retorting (heating) allowing access to liquid oil (Grady and Kipp, 1987). Strain rates applied to the rock during these experiments ranged from  $10^0$  to  $10^4 \text{ s}^{-1}$  bracketing the range of rates typically applied during blasting events (Grady and Kipp, 1987). The relationship derived by Grady and Kipp (1987) was most recently applied by Reches and Dewers (2005) in their study of dynamic fracture along fault zones. This relationship is given by

$$d = \left[ \frac{(\sqrt{20}K_{IC})^2}{\rho C_d \dot{\varepsilon}} \right]^{\frac{2}{3}} \quad (1)$$

where  $d$  is the diameter of the fragmented grains,  $K_{IC}$  is the mode I fracture toughness of the unfractured grain,  $\rho$  is the rock density,  $C_d$  is the compressive (P-wave) velocity of the Navajo Sandstone, and  $\dot{\varepsilon}$  is the strain rate applied to the rock at the time of faulting.

Zhou et al. (2005) re-evaluated Grady and Kipp's (1987) relationship between grain size and strain rate by comparing data generated from 1 dimensional (1D) armor ceramic system models to the data presented by Grady and Kipp. The comprehensive model presented by Zhou et al. (2005) took a numerical approach to the evaluation of dynamic fragmentation, considering a wide range of strain rates ( $10^1$  to  $5 \times 10^6 \text{ s}^{-1}$ ) and

incorporated various spatial distributions of intrinsic defects and material strengths. Zhou et al. (2005) also incorporated elastic wave interaction with cohesive crack opening resulting in a prediction of the number of fragments a rock will break into under a given strain rate. Grain sizes calculated from these simulations, in which original grains with randomly oriented flaws were subjected to high strain rate conditions (defined as  $\geq 10^3 \text{ s}^{-1}$ ), revealed that grain sizes are reduced by approximately 40% compared to those predicted by Grady and Kipp (1987) (Zhou et al., 2005). At low (quasi-static) strain rates ( $\leq 10^1 \text{ s}^{-1}$ ) where only a portion of the strain energy goes towards the development of new cracks, fragment sizes are not dependent on strain rate and a constant fragment grain size is predicted (Zhou et al., 2005). Applying rock properties appropriate to the Navajo Sandstone (discussed below), we predict a linear strain rate to grain size relationship for strain rates  $\geq 10^{-1} \text{ s}^{-1}$  with constant grain sizes of approximately  $4 \times 10^{-2} \text{ m}$  predicted at strain rates  $\leq 10^{-7} \text{ s}^{-1}$  as shown in Figure 8. We also define a parameter,  $f$ , which accounts for the shift in values obtained by Grady and Kipp's relation (1987) as suggested by Zhou et al. (2005). Adjusted to reflect this shift and rearranged for strain rate, Grady and Kipp's equation (1987) is given by

$$\dot{\varepsilon} = \frac{\sqrt{20}K_{IC}}{\rho C_d \left(\frac{d}{f}\right)^{\frac{3}{2}}} \quad (2)$$

where  $f = 1$  in Grady and Kipp's original equation (1987) and  $f = 0.4$  following Zhou et al. (2005). We prefer strain rates obtained from Grady and Kipp's (1987) adjusted relationship (Equation 2), where  $f = 0.4$ .

We apply the adjusted Grady and Kipp (1987) relation (Equation 2) to the samples of pulverized rock obtained from the field locations at Upheaval Dome in order to estimate strain rates along the faults at the time of impact. We measured grain sizes from fragmented grains observed in thin sections (for example Figure 6) and plotted these as a function of strain rate as shown in Figure 8 using Equation 2. Along with measured grain sizes of  $3.75 \times 10^{-6}$  m to  $1.40 \times 10^{-4}$  m, we chose values of  $K_{IC}$  of 10-100  $\text{MPa} \cdot \text{m}^{1/2}$ , which brackets the  $30 \text{ MPa} \cdot \text{m}^{1/2}$  used by Reches and Dewers (2005) by one order of magnitude,  $\rho$  of  $2,250 \text{ kg/m}^3$  appropriate to undeformed Navajo Sandstone (Sternlof et al., 2005; value obtained from the Aztec Sandstone which is correlative with the Navajo Sandstone [Marzolf, 1983]), and  $C_d$  of 2,483 m/s obtained using

$$C_d = \sqrt{\frac{\mu + \lambda}{\rho}} \quad (3)$$

(Reches and Dewers, 2005). Values were obtained for Lamé's coefficient ( $\lambda$ ) and the shear modulus ( $\mu$ ) using

$$\lambda = \frac{E\nu}{(1+\nu)(1-2\nu)} \quad (4)$$

$$\mu = \frac{E}{2(1+\nu)} \quad (5)$$

(Timoshenko and Goodier, 1970), with Young's modulus ( $E$ ) of 20 GPa and Poisson's ratio ( $\nu$ ) of 0.2 (Sternlof et al., 2005) appropriate to the Navajo Sandstone.

Using a representative measured grain size of  $4 \times 10^{-5}$  m for pulverized rock observed along faults at Upheaval Dome in Equation 2 with  $f = 1$  (Grady and Kipp, 1987), we obtain a strain rate of  $88 \text{ s}^{-1}$ . Using maximum and minimum measured grain sizes of  $3.75 \times 10^{-6}$  to  $1.40 \times 10^{-4}$  m, strain rates ranging from 5 to  $1 \times 10^4 \text{ s}^{-1}$  are obtained. Using  $f = 0.4$ , we obtain a representative strain rate of  $2 \times 10^1 \text{ s}^{-1}$  for faulting at Upheaval Dome, with strain rates ranging from 1 to  $3 \times 10^3 \text{ s}^{-1}$  using maximum and minimum measured grain sizes. Results are presented in Figure 8 with the dashed line on the right side of the plot representing  $K_{IC} = 100 \text{ MPa} \cdot \text{m}^{1/2}$  for  $f = 1$  and the solid lines representing  $K_{IC}$  ranging from  $10 \text{ MPa} \cdot \text{m}^{1/2}$  to  $100 \text{ MPa} \cdot \text{m}^{1/2}$  following Reches and Dewers (2005) for  $f = 0.4$ .

To compare strain rates calculated along faults within Upheaval Dome to rates generated elsewhere, strain rates associated with the pulverization of sedimentary rocks documented and studied along the Mojave section of the San Andreas Fault in southern California (Dor et al., 2009) were also calculated. Doan and Gary (2008) estimated strain rates responsible for generating pulverized rock along the San Andreas Fault of at least  $1.5 \times 10^{-2} \text{ s}^{-1}$  using high strain rate laboratory testing methods. Using grain sizes ranging from  $2.56 \times 10^{-3}$  to  $1.51 \times 10^{-4}$  m obtained by Dor et al. (2009) for pulverized sedimentary rocks along the San Andreas Fault and Grady and Kipp's (1987) relationship (Equation 2, with  $f = 1$ ), we obtain maximum and minimum strain rates ranging from  $6 \times 10^{-2}$  to  $4 \times 10^1 \text{ s}^{-1}$ . Using  $f = 0.4$ , we obtain strain rates ranging from  $2 \times 10^{-2}$  to  $2 \times 10^1 \text{ s}^{-1}$ .

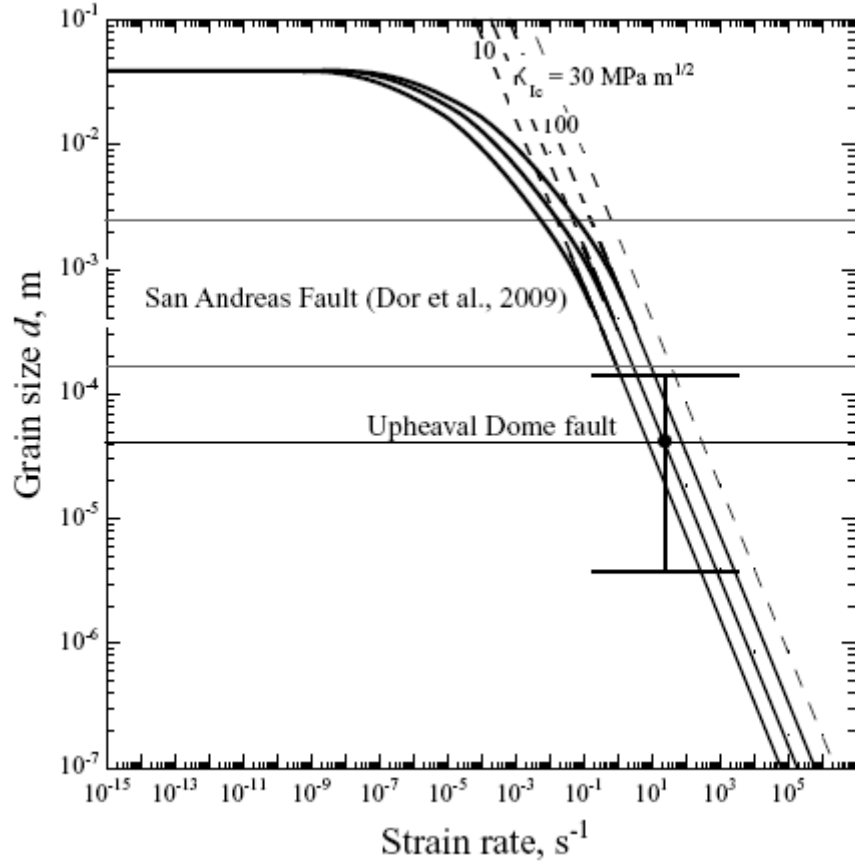


Figure 8: Plot of measured pulverized grain sizes and corresponding strain rates for data collected along faults at Upheaval Dome (this work) and the sedimentary rocks along the San Andreas Fault (Dor et al., 2009). Equation 2, where  $f = 1$  (from Grady and Kipp, 1987) with a  $K_{IC}$  of 100 MPa has been plotted as a dashed line in on the right hand side of the figure for comparison to Equation 2, where  $f = 0.4$  (following Zhou et al., 2005) plotted as solid lines.

We find that strain rates calculated for faults at Upheaval Dome ( $1$  to  $3 \times 10^3 \text{ s}^{-1}$ ) remain larger in magnitude than strain rates calculated along the Mojave section of the San Andreas Fault ( $2 \times 10^{-2}$  to  $2 \times 10^1 \text{ s}^{-1}$ ). The strain rates calculated for pulverized rock at Upheaval Dome and the San Andreas Fault exceed those typically reported in the literature for intraplate tectonics (i.e. tectonic deformation occurring with distance from active tectonic margins or plate boundaries) which range from  $10^{-20}$  to  $10^{-17} \text{ s}^{-1}$  (Gordon, 1998) as well as those used in standard uniaxial and triaxial laboratory experiments (e.g.

ASTM Standard D7012, 2004). Strain rates we have calculated for Upheaval Dome are up to 20 orders of magnitude larger than the highest strain rates generated in intraplate tectonic settings. Our findings suggest that there is a rate-dependence for faulting in porous sedimentary rocks with DBDZs developing in response to strain rates  $< 10^{-2} \text{ s}^{-1}$  and pulverized rock forming in response to strain rates  $\geq 10^{-2} \text{ s}^{-1}$ .

According to Wilson et al. (2005), rock pulverization is a function of strain rate and velocity resulting from a single earthquake event but not a function of cumulative slip. Zones of pulverized rock are observed to approach 100 to 200 meters in thickness along the Mojave section of the San Andreas Fault (Brune, 2001; Dor et al., 2006, 2009) where fault offset is on the order of tens to hundreds of kilometers (Wilson et al., 2005). By contrast, zones of pulverized rock observed along faults located within the rim syncline in this study are several centimeters in thickness. Maximum fault offsets within the rim syncline at Upheaval Dome where the faults evaluated in this study are located are estimated to be on the order of meters to tens of meters (Kenkmann et al., 2005). It appears that the width of pulverized zones is related to the amount of fault offset.

## CONCLUSIONS

We find that faulting in the porous Navajo Sandstone within the rim syncline of Upheaval Dome is accommodated by the formation of selectively pulverized rock along fault planes and not by the formation of DBDZs, as observed elsewhere on the Colorado Plateau outside the impact structure. Using the relationships obtained by Grady and Kipp (1987) and Zhou et al. (2005), we find that these faults formed in response to strain rates ranging from 1 to  $3 \times 10^3 \text{ s}^{-1}$ . Our findings indicate that at strain rates of  $10^{-2} \text{ s}^{-1}$  and greater

cracking-dominated deformation (i.e. pulverization) occurs in the Navajo Sandstone, and at strain rates less than  $10^{-2} \text{ s}^{-1}$  compaction-dominated deformation (i.e. deformation bands and DBDZs) occurs. We also infer that strain rates ranging from  $6 \times 10^{-2}$  to  $2 \times 10^1 \text{ s}^{-1}$  were generated during dynamic earthquake events along the Mojave section of the San Andreas Fault. Our results further support the conclusion that Upheaval Dome formed in response to a meteorite impact.

Our findings provide additional insight into fault formation. Pulverized rock has been documented in all rock types (i.e. sedimentary, crystalline, and metamorphic) where faulting is observed. We suggest that detailed mapping and evaluations of faults formed in response to terrestrial impact cratering events may yield additional occurrences of pulverized rock providing an additional independent criterion for identifying potential terrestrial impact craters. Because faulting is more prevalent within complex craters as opposed to simple craters, we anticipate additional evidence for pulverized rock is more likely to be found along faults within preserved complex craters. Understanding strain rate conditions at an impact site provides a new source of information regarding the mechanical responses of rock types affected by deformation at impact strain rates. Impact craters, such as Upheaval Dome, where faults are radial and display greater offsets at the center of the crater than at the crater rims, may provide ideal locations for testing the relationship fault offsets to the widths of pulverized zones.

## REFERENCES

- Alvarez, W., Staley, E., O'Connor, D., and Chan, M., 1998, Synsedimentary deformation in the Jurassic of southern Utah- a case of impact shaking: *Geology*, v. 26, p. 579-582.
- An, L.J. and Sammis, C.G., 1994, Particle size distribution of cataclastic fault materials from Southern California: A 3-D study, *in* Marone, C.J. and Blanpied, M.L., eds., *Faulting, friction, and earthquake mechanics Part II*, Pure and Applied Geophysics Topical Volumes, v. 143, no. 1-3, p. 203-227.
- Antonellini, M.A., Aydin, A., and Pollard, D.P., 1994, Microstructure of deformation bands in porous sandstones at Arches National Park, Utah: *Journal of Structural Geology*, v. 16, no. 7, p. 941-959.
- Ashworth, J.R. and Schneider, H., 1985, Deformation and transformation in experimentally shock-loaded quartz: *Physics and Chemistry of Minerals*, no. 11, p. 241-249.
- ASTM Standard D7012, 2004 (2006), Standard test method for compressive strength and elastic moduli of intact rock and core specimens under varying states of stress and temperature: ASTM International, West Conshohocken, PA, 2006, DOI: 10.1520/D7012-04, [www.astm.org](http://www.astm.org).
- Aydin, A., 1978, Small faults formed as deformation bands in sandstone: *Pure and Applied Geophysics*, v. 116, no. 4-5, p. 913-930.
- Aydin, A. and Johnson, A.M., 1978, Development of faults as zones of deformation bands and as slip surfaces in sandstone: *Pure and Applied Geophysics*, v. 116, no. 4-5, p. 931-942.
- Aydin, A. and Johnson, A.M., 1983, Analysis of faulting in porous sandstones: *Journal of Structural Geology*, v. 5, no. 1, p. 19-31.
- Aydin, A., Borja, R.I., and Eichhubl, P., 2006, Geological and mathematical framework for failure modes in granular rock: *Journal of Structural Geology*, v. 28, no. 1, p. 83-98.
- Brune, J.N., 2001, Fault normal dynamic loading and unloading: an explanation for "nongouge" rock powder and lack of fault parallel shear bands along the San Andreas fault [abs.]: *Eos (Transaction, American Geophysical Union)*, v. 82, no. 47.
- Buchner, E. and Kenkmann, T., 2008, Upheaval Dome, Utah, USA: Impact origin confirmed: *Geological Society of America Bulletin*, v. 36, no. 3, p. 227-230.

- Crider, J.G. and Peacock, D.C.P., 2004, Initiation of brittle faults in the upper crust: A review of field observations: *Journal of Structural Geology*, v. 26, p. 691-707.
- Davis, G.H., 1999, Structural geology of the Colorado Plateau region of southern Utah with special emphasis on deformation bands: *Geological Society of America Special Paper 342*, 157 p.
- Davis, G.H., Bump, A.P., Garcíá, P.E., and Ahlgren, S.G., 1999, Conjugate Riedel deformation band shear zones: *Journal of Structural Geology*, v. 22, p. 169-190.
- Doan, M. and Gary, G., 2008, Rocks pulverized near San Andreas Fault: Insight from high strain rate testing experiments [abs.]: *Eos (Transaction, American Geophysical Union)*, v. 89, no. 53.
- Dor, O., Ben-Zion, Y., Rockwell, T.K., and Brune, J., 2006, Pulverized rocks in the Mojave section of the San Andreas Fault Zone: *Earth and Planetary Science Letters*, v. 245, p. 642-654.
- Dor, O., 2007, Symmetry properties, pulverized rocks and damage architecture in fault zones as signatures of earthquake ruptures [Ph.D. thesis]: University of Southern California, 293 p.
- Dor, O., Chester, J.S., Ben-Zion, Y., Brune, J.N., Rockwell, T.K., 2009, Characterization of damage in sandstones along the Mojave section of the San Andreas Fault: Implications for the shallow extent of rock pulverization: *Pure and Applied Geophysics*, in press.
- Engelder, J.T., 1974, Cataclasis and the formation of fault gouge: *Geological Society of America Bulletin*, v. 85, p. 1515-1522.
- Fiero, W.G., Jr., 1958, Geology of Upheaval Dome, San Juan County, Utah [Master's thesis]: Laramie, University of Wyoming, 85 p.
- Fossen, H., Schultz, R.A., Shipton, Z.K., and Mair, K., 2007, Deformation bands in sandstone: A review: *Journal of the Geological Society, London*, v. 164, p. 755-769.
- Fossum, A.F. and Brannon, R.M., 2006, On a viscoplastic model for rocks with mechanism-dependent characteristic times: *Acta Geotechnica*, v. 1, p. 89-106.
- French, B.M., 1998, Traces of catastrophe: A handbook of shock-metamorphic effects in terrestrial meteorite impact structures: *Lunar and Planetary Institute Contribution No. 954*, Lunar and Planetary Institute, Houston, 120 p.

- Gordon, R.G., 1998, The plate tectonic approximation: Plate nonrigidity, diffuse plate boundaries, and global plate reconstructions: *Annual Review of Earth and Planetary Science*, v. 26, p. 615-642.
- Grady, D.E. and Kipp, M.E., 1987, Dynamic rock fragmentation, *in* Atkinson, B.K., ed., *Fracture Mechanics of Rock*, Academic Press, p. 429-475.
- Gratz, A.J., Tyburezy, J., Christie, J., Ahrens, T., Pongratz, P., 1988, Shock metamorphism of deformed quartz: *Physics and Chemistry of Minerals*, no. 16, p. 221-233.
- Grieve, R.A.F., 1991, Terrestrial impact: The record in the rocks: *Meteoritics*, v. 26, p. 175-194.
- Grieve, R.A.F., and Therriault, A.M., 2003, Observations at terrestrial impact structures: Their utility in constraining crater formation: *Meteoritics and Planetary Science*, v. 39, no. 2, p. 199-216.
- Gu, Y. and Wong, T.F., 1994, Development of shear localization in simulated quartz gouge: Effect of cumulative slip and gouge particle size, *in* Marone, C.J. and Blanpied, M.L., eds., *Faulting, friction, and earthquake mechanics Part II*, *Pure and Applied Geophysics Topical Volumes*, v. 143, no. 1-3, p. 387-423.
- Harrison, T.S., 1927, Colorado-Utah salt domes: *Bulletin of the American Association of Petroleum Geologists*, vol. 11, no. 2, pp.111-133.
- Huntoon, P.W., 2000, Upheaval Dome, Canyonlands, Utah: Strain indicators that reveal an impact origin, *in* Sprinkel, D.A., Chidsey, Jr., T.C., and Anderson, B.P., eds., *Geology of Utah's Parks and Monuments*, Utah Geological Association Publication 28.
- Holcomb, D., Rudnicki, J.W., Issen, K.A., and Sternlof, K., 2007, Compaction localization in the Earth and laboratory: State of the research and research directions: *Acta Geotechnica*, v. 2, p. 1-15.
- Jackson, M.P.A., Schultz-Ela, D.D., Hudec, M.R., Watson, I.A., and Porter, M.L., 1998, Structure and evolution of Upheaval Dome: A pinched-off salt diapir: *Geological Society of America Bulletin*, v. 110, no. 12, p. 1547-1573.
- Kanbur, Z., Louie, J.N., Chavez-Perez, S. Plank, G., and Morey, D., 1999, Seismic reflection study of Upheaval Dome, Canyonlands National Park, Utah: *Journal of Geophysical Research*, v. 105, no. E4, p. 9489-9505.
- Kenkmann, T., 2003, Dike formation, cataclastic flow, and rock fluidization during impact cratering: An example from the Upheaval Dome structure, Utah: *Earth and*

Planetary Science Letters, v. 214, p. 43-58.

- Kenkmann, T., Jahn, A., Scherler, D., and Ivanov, B.A., 2005, Structure and formation of a central uplift: A case study at Upheaval Dome impact crater, Utah, *in* Kenkmann, T., Horz, F., and Deutsch, A., eds., Large Meteorite Impacts III, Geological Society of America Special Paper 384, p. 85-115.
- Kriens, B.J., Shoemaker, E.M., and Herkenhoff, K.E., 1997, Structure and kinematics of a complex impact crater, Upheaval Dome, southeast Utah, *in* Link, P.K., and Kowallis, B.J., eds., Geological Society of America Field Trip Guidebook, vol. 42, p. 19-31.
- Kriens, B.J., Shoemaker, E.M., and Herkenhoff, K.E., 1999, Geology of the Upheaval Dome impact structure, southeast Utah: *Journal of Geophysical Research*, v. 104, no. E8, p. 18,867-18,887.
- Lockner, D.A., Byerlee, J.D., Kuksenko, V., Ponomarev, A., and Sidorin, A., 1991, Quasi-static fault growth and shear fracture energy in granite: *Nature*, v. 350, p. 39-42.
- Lockner, D.A., 1995, Rock failure, *in* Ahrens, T.J., ed, Rock physics and phase relations- A handbook of physical constants, American Geophysical Union Reference Shelf 3, p. 127-147.
- Louie, J. N., Chavez-Perez, S., and Plank, G., 1995, Impact deformation at Upheaval Dome, Canyonlands National Park, Utah, revealed by seismic profiles [abs.]: *Eos* (Transactions, American Geophysical Union), v. 76, no. 46.
- Martel, S.J. and Pollard, D.D., 1989, Mechanics of slip and fracture along small faults and simple strike-slip fault zones in granitic rock: *Journal of Geophysical Research*; v. 94, p. 9,417-9,428.
- Marzolf, J.E., 1983, Changing wind and hydrologic regimes during deposition of the Navajo and Aztec sandstones, Jurassic (?), southwestern United States, *in* Brookfield, M.E. and Ahlbrandt, T.S., eds., Eolian Sediments and Processes, Developments in Sedimentology, vol. 38, New York, Elsevier, p. 635-660.
- Mattox, R.B., 1968, Upheaval Dome, a possible salt dome in the Paradox Basin, Utah, *in* Mattox, R.B., ed., Saline deposits: Geological Society of America Special Paper 88, p. 331-347.
- Mattox, R.B., 1975, Upheaval Dome, a possible salt dome in the Paradox Basin, Utah, *in* Fassett, J.E. and Wengerd, S.A., eds., Canyonlands Country: A Guidebook of the Four Corners Geological Society, Eighth Field Conference, p. 225-234.

- McKnight, E.T., 1940, Geology of area between Green and Colorado Rivers, Grand and San Juan Counties, Utah: United States Geological Survey Bulletin 908, 147 p.
- Melosh, H.J. and Gaffney, E.S., 1983, Acoustic fluidization and the scale dependence of impact crater morphology: *Journal of Geophysical Research*, v. 88 B2, p. A830-A834.
- Melosh, H.J., 1989, Impact cratering: A geologic process: Oxford Monographs on Geology and Geophysics No. 11, New York, Oxford University Press, 245 p.
- Molenaar, C.M., 1975, Lexicon of stratigraphic names used in the Paradox Basin-San Rafael-Henry Mountains area, Utah, *in* Fassett, J.E. and Wengerd, S.A., eds., Canyonlands Country: A Guidebook of the Four Corners Geological Society, Eighth Field Conference, p. 5-11.
- Morgan, J. and Warner, M., 1999, Morphology of Chicxulub impact: Peak-ring crater or multi-ring basin? *in* Dressler, B.O. and Sharpton, V.L., eds., Large meteorite impacts and planetary evolution; II, Geological Society of America Special Paper 339, p. 281-290.
- Okubo, C. and Schultz, R.A., 2005, Evolution of damage zone geometry and intensity in porous sandstone: Insight gained from strain energy density: *Journal of the Geological Society, London*, v. 162, p. 939-949.
- Okubo, C.H. and Schultz, R.A., 2007, Compactional deformation bands in Wingate Sandstone; additional evidence of an impact origin for Upheaval Dome, Utah: *Earth and Planetary Science Letters*, v. 256, p. 169-181.
- Osinski, G.R., Lee, P., Spray, J.G., Parnell, J., Lim, D.S.S., Bunch, T.E., Cockell, C.S., and Glass, B., 2005, Geological overview and cratering model for the Haughton impact structure, Devon Island, Canadian High Arctic: *Meteoritics and Planetary Science*, v. 40, n. 12, p. 1,759-1,776.
- Osinski, G.R. and Spray, J.G., 2005, Tectonics of complex crater formation as revealed by the Haughton impact structure, Devon Island, Canadian High Arctic: *Meteoritics and Planetary Science*, v. 40, n. 12, p. 1,813-1,834.
- Paterson, M.S. and Wong, T.F., 2005, *Experimental Rock Deformation- The Brittle Field*, 2<sup>nd</sup> Ed., Berlin, Springer, 348 p.
- Pati, J.K. and Reimold, W.U., 2007, Impact cratering-Fundamental process in geoscience and planetary science: *Journal of Earth System Science*, v. 116, no. 2, p. 81-98.
- Prakash, V., Yuan, F., Dor, O., Tullis, T., and Goldsby, D., 2008, Laboratory investigations of the origin of pulverized rocks [abs.]: *Eos (Transactions)*,

- American Geophysical Union), v. 89, no. 53.
- Reches, Z. and Dewers, T.A., 2005, Gouge formation by dynamic pulverization during earthquake rupture: *Earth and Planetary Science Letters*, v. 235, p. 361-374.
- Sagy, A., Reches, Z., and Fineberg, J., 2002, Dynamic fracture by large extraterrestrial impacts as the origin of shatter cones: *Nature*, v. 418, p. 310-313.
- Sagy, A., Fineberg, J., Reches, Z., 2004, Shatter cones: Branched, rapid fractures formed by shock impact: *Journal of Geophysical Research*, v. 109, no. B10209, p. 1-20.
- Sammis, C.G., King, G.C.P., and Biegel, R., 1987, The kinematics of gouge deformation: *Pure and Applied Geophysics*, v. 125, p. 777-812.
- Sammis, C.G. and Steacy, S.J., 1995, Fractal fragmentation in crustal shear zones, *in* Barton, C.C. and La Pointe, P.R., eds., *Fractals in the Earth Sciences*, New York, Plenum Press, p. 179-204.
- Sammis, C.G. and King, G.C.P., 2007, Mechanical origin of power law scaling in fault zone rock: *Geophysical Research Letters*, v. 34, no. L04312, p. 1-4.
- Scherler, D., Kenkmann, T., and Jahn, A., 2006, Structural record of an oblique impact: *Earth and Planetary Science Letters*, v. 248, p. 43-53.
- Schultz, R.A. and Balasko, C.M., 2003, Growth of deformation bands into echelon and ladder geometries: *Geophysical Research Letters*, v. 30, no. 20, p. 2033-2037.
- Schultz, R.A. and Siddharthan, R., 2005, A general framework for the occurrence and faulting of deformation bands in porous granular rocks: *Tectonophysics*, v. 411, p. 1-18.
- Schultz, R.A. and Fossen, H., 2008, Terminology for structural discontinuities: *American Association of Petroleum Geologists Bulletin*, v. 92, p. 853-867.
- Schultz-Ela, D.D., Jackson, M.P.A., Hudec, M.R., Fletcher, R.C., Porter, M.L., and Watson, I.A., 1994, Structures formed by radial contraction at Upheaval Dome, Utah [abs]: *Geological Society of America Abstracts with Programs*, v. 26.
- Segall, P. and Pollard, D.D., 1983, Nucleation and growth of strike-slip faults in granite: *Journal of Geophysical Research*, v. 88, p. 555-568.
- Shipton, Z.K. and Cowie, P., 2001, Damage zone and slip surface evolution of  $\mu\text{m}$  to km scales in high-porosity Navajo Sandstone: *Journal of Structural Geology*, v. 23, no. 3, p. 1825-1844.

- Shipton, Z.K. and Cowie, P., 2003, A conceptual model for the origin of fault damage zone structures in high-porosity sandstones: *Journal of Structural Geology*, v. 25, no. 12, p. 333-344.
- Shoemaker, E.M., 1960, Penetration mechanics of high velocity meteorites, illustrated by Meteor Crater, Arizona: International Geological Congress, Representative Session, Norden, 21<sup>st</sup>, Part 18, p. 418-434.
- Shoemaker, E.M. and Herkenhoff, K.E., 1983, Impact origin of Upheaval Dome, Utah [abs.]: *Eos (Transactions, American Geophysical Union)*, v. 64.
- Spray, J.G., 1997, Superfaults: *Geology*, v. 25, no. 7, p. 579-582.
- Sternlof K.R., Rudnicki, J.W., and Pollard, D.D., 2005, Anticrack inclusion model for compaction bands in sandstone: *Journal of Geophysical Research*, vol. 110, no. B11403, p. 1-16.
- Timoshenko, S.P. and Goodier, J.N., 1970, *Theory of elasticity*: New York, McGraw-Hill, 567 p.
- Torabi, A., Braathen, A., Cuisiat, F., and Fossen, H., 2007, Shear zones in porous sands: Insights from ring-shear experiments and naturally deformed sandstones: *Tectonophysics*, v. 437, p. 37-50.
- Wawersik, W.R. and Brace, W.F., 1971, Post-failure behavior of a granite and diabase: *Rock Mechanics*, v. 3, p. 61-85.
- Wawersik, W.R. and Fairhurst, C., 1970, A study of brittle rock fracture in laboratory compression experiments: *International Journal of Rock Mechanics and Mining Sciences*, v. 7, p. 561-575.
- Wilson, B., Dewers, T., Reches, Z., and Brune, J., 2005, Particle size and energetics of gouge from earthquake rupture zones: *Nature*, v. 434, p. 749-752.
- Woodward-Clyde Consultants, 1983, Overview of the regional geology of the Paradox basin study region: Columbus, Ohio, Office of Nuclear Waste Isolation Technical Report ONWI-92, 433 p.
- Zhou, F., Molinari, J.F., and Ramesh, K.T., 2005, A cohesive model based fragmentation analysis: Effects of strain rate and initial defects distribution: *International Journal of Solids and Structures*, v. 42, p. 5,181-5,207.

## APPENDIX 1: GRAIN SIZE MEASUREMENTS

This appendix provides grain size measurements and calculations made from thin sections obtained from pulverized rock material along Fault 1 (see Figures 2, 4, and 5). The first table is a compilation of measurements of the individual pulverized/ fractured grains. In order to compare the pulverized grain sizes to the original grain sizes prior to faulting and pulverization, the second table is a compilation of measurements of the original quartz grains. These measurements were possible because the rock's original fabric was maintained after pulverization thus preserving original grain boundaries in contrast to fault gouge in which grains are sheared. In each case, the left column represents the numbers of grains measured ( $n$ , unitless), the middle columns display length ( $l_1$ ) and width ( $l_2$ ) data measured directly from thin section images (in mm), and the right column presents the calculated grain size ( $d$ , in mm) obtained from the equation

$$d = \frac{l_1 + l_2}{2} \quad (A1)$$

The average grain sizes for the pulverized material and the original grains are reported at the bottom of Tables A1 and A2 respectively.

Table A1: Pulverized Rock Grain Size Data

<i>n</i>	<i>l</i> <sub>1</sub> (mm)	<i>l</i> <sub>2</sub> (mm)	<i>d</i> (mm)
1	0.9	0.055	0.4775
2	0.32	0.17	0.245
3	0.16	0.12	0.14
4	0.22	0.03	0.125
5	0.16	0.09	0.125
6	0.14	0.1	0.12
7	0.14	0.1	0.12
8	0.15	0.1	0.12
9	0.16	0.06	0.11
10	0.13	0.09	0.11
11	0.13	0.09	0.11
12	0.16	0.04	0.1
13	0.15	0.05	0.1
14	0.1	0.1	0.1
15	0.14	0.005	0.095
16	0.11	0.07	0.09
17	0.12	0.05	0.085
18	0.12	0.04	0.08
19	0.11	0.05	0.08
20	0.1	0.05	0.08
21	0.09	0.06	0.075
22	0.08	0.06	0.07
23	0.11	0.03	0.07
24	0.1	0.04	0.07
25	0.08	0.06	0.07
26	0.08	0.06	0.07
27	0.08	0.06	0.07
28	0.12	0.01	0.065
29	0.9	0.04	0.065
30	0.08	0.05	0.065
31	0.07	0.06	0.065
32	0.07	0.06	0.065
33	0.07	0.05	0.06
34	0.09	0.03	0.06
35	0.09	0.03	0.06
36	0.06	0.06	0.06
37	0.07	0.04	0.055
38	0.08	0.03	0.055
39	0.08	0.03	0.055
40	0.06	0.05	0.055
41	0.06	0.05	0.055

Table A1: Pulverized Rock Grain Size Data Continued

<i>n</i>	<i>l</i> <sub>1</sub> (mm)	<i>l</i> <sub>2</sub> (mm)	<i>d</i> (mm)
42	0.06	0.05	0.055
43	0.06	0.05	0.05
44	0.08	0.02	0.05
45	0.07	0.02	0.045
46	0.07	0.02	0.045
47	0.07	0.02	0.045
48	0.07	0.02	0.045
49	0.06	0.02	0.04
50	0.06	0.02	0.04
51	0.05	0.03	0.04
52	0.05	0.03	0.04
53	0.05	0.03	0.04
54	0.05	0.03	0.04
55	0.05	0.03	0.04
56	0.05	0.03	0.04
57	0.04	0.04	0.04
58	0.05	0.025	0.0375
59	0.05	0.02	0.035
60	0.05	0.02	0.035
61	0.05	0.02	0.035
62	0.05	0.02	0.035
63	0.045	0.025	0.035
64	0.04	0.03	0.035
65	0.04	0.03	0.035
66	0.04	0.03	0.035
67	0.04	0.03	0.035
68	0.04	0.03	0.035
69	0.04	0.03	0.035
70	0.06	0.01	0.035
71	0.045	0.02	0.0325
72	0.045	0.02	0.0325
73	0.04	0.025	0.0325
74	0.04	0.02	0.03
75	0.04	0.02	0.03
76	0.04	0.02	0.03
77	0.04	0.02	0.03
78	0.04	0.02	0.03
79	0.03	0.03	0.03
80	0.04	0.01	0.025
81	0.03	0.02	0.025
82	0.03	0.02	0.025

Table A1: Pulverized Rock Grain Size Data Continued

<i>n</i>	<i>l</i> <sub>1</sub> (mm)	<i>l</i> <sub>2</sub> (mm)	<i>d</i> (mm)
83	0.03	0.02	0.025
84	0.03	0.02	0.025
85	0.03	0.02	0.025
86	0.03	0.02	0.025
87	0.03	0.02	0.025
88	0.03	0.01	0.02
89	0.03	0.01	0.02
90	0.025	0.015	0.02
91	0.02	0.02	0.02
92	0.02	0.02	0.02
93	0.02	0.02	0.02
94	0.02	0.015	0.0175
95	0.02	0.015	0.0175
96	0.02	0.015	0.0175
97	0.02	0.015	0.0175
98	0.02	0.015	0.0175
99	0.025	0.005	0.015
100	0.02	0.01	0.015
101	0.02	0.01	0.015
102	0.02	0.01	0.015
103	0.02	0.01	0.015
104	0.02	0.01	0.015
105	0.02	0.01	0.015
106	0.02	0.01	0.015
107	0.02	0.01	0.015
108	0.02	0.01	0.015
109	0.02	0.01	0.015
110	0.02	0.01	0.015
111	0.02	0.01	0.015
112	0.02	0.01	0.015
113	0.02	0.01	0.015
114	0.02	0.01	0.015
115	0.02	0.01	0.015
116	0.02	0.01	0.015
117	0.02	0.01	0.015
118	0.015	0.015	0.015
119	0.02	0.005	0.0125
120	0.02	0.005	0.0125
121	0.015	0.01	0.0125
122	0.015	0.01	0.0125
123	0.015	0.01	0.0125

Table A1: Pulverized Rock Grain Size Data Continued

<i>n</i>	<i>l<sub>1</sub></i> (mm)	<i>l<sub>2</sub></i> (mm)	<i>d</i> (mm)
124	0.015	0.005	0.01
125	0.015	0.005	0.01
126	0.015	0.005	0.01
127	0.01	0.01	0.01
128	0.01	0.01	0.01
129	0.01	0.01	0.01
130	0.01	0.01	0.01
131	0.01	0.01	0.01
132	0.015	0.0025	0.00875
133	0.01	0.005	0.0075
134	0.01	0.005	0.0075
135	0.01	0.005	0.0075
136	0.01	0.005	0.0075
137	0.01	0.005	0.0075
138	0.01	0.005	0.0075
139	0.01	0.005	0.0075
140	0.01	0.0025	0.00625
141	0.005	0.005	0.005
142	0.005	0.005	0.005
143	0.005	0.005	0.005
144	0.005	0.005	0.005
145	0.005	0.005	0.005
146	0.005	0.0025	0.00375
147	0.005	0.0025	0.00375
148	0.005	0.0025	0.00375

Average pulverized grain size:  $0.04 \pm 0.4$  mm

Table A2: Original Grain Size Data

<i>n</i>	<i>l<sub>1</sub></i> (mm)	<i>l<sub>2</sub></i> (mm)	<i>d</i> (mm)
1	0.0475	0.44	0.4575
2	0.04	0.325	0.3625
3	0.55	0.03	0.29
4	0.33	0.21	0.27
5	0.45	0.04	0.245
6	0.22	0.15	0.185
7	0.15	0.11	0.13
8	0.14	0.11	0.125
9	0.15	0.09	0.12
10	0.14	0.085	0.1125
11	0.135	0.07	0.1025
12	0.08	0.06	0.07
13	0.07	0.06	0.065
14	0.07	0.06	0.065
15	0.08	0.035	0.0575
16	0.07	0.04	0.055
17	0.07	0.03	0.05
18	0.045	0.04	0.0425
19	0.055	0.03	0.0425
20	0.05	0.03	0.04
21	0.05	0.03	0.04
22	0.06	0.02	0.04
23	0.05	0.025	0.0375
24	0.05	0.02	0.035
25	0.05	0.02	0.035
26	0.04	0.02	0.03
27	0.035	0.02	0.0275
28	0.03	0.025	0.0275
29	0.025	0.025	0.025
30	0.025	0.02	0.0225
31	0.03	0.015	0.0225
32	0.03	0.01	0.02
33	0.025	0.015	0.02
34	0.02	0.015	0.0175
35	0.02	0.01	0.015
36	0.02	0.01	0.015
37	0.015	0.01	0.0125
38	0.015	0.01	0.0125
39	0.015	0.01	0.0125
40	0.01	0.01	0.01
41	0.01	0.01	0.01

Table A2: Original Grain Size Data Continued

<b><i>n</i></b>	<b><i>l<sub>1</sub></i> (mm)</b>	<b><i>l<sub>2</sub></i> (mm)</b>	<b><i>d</i> (mm)</b>
42	0.01	0.01	0.01
43	0.01	0.005	0.0075
44	0.01	0.005	0.0075
45	0.01	0.005	0.0075
46	0.01	0.005	0.0075

Average original grain size:  $0.07 \pm 0.4$  mm